The 9th European Congress on Computational Methods in Applied Sciences and Engineering
ECCOMAS Congress 2024
3–7 June 2024, Lisboa, Portugal

ALMOST PERIODIC FOURIER TRANSFORMATIONS FOR THE ANALYSIS OF PERIODIC PHENOMENA IN TURBOMACHINERY

JENS WELLNER[1], GRAHAM ASHCROFT[1] AND DANIEL SCHLÜß[2]

[1] Institute of Propulsion Technology
German Aerospace Center (DLR)
Linder Höhe, Cologne 51147, Germany
e-mail: jens.wellner@dlr.de, graham.ashcroft@dlr.de, www.dlr.de/en

[2] MTU Aero Engines AG
Dachauer Straße 665, 80995 Munich, Germany
email: daniel.schluess@mtu.de, www.mtu.de

Key words: Almost Periodic Fourier Transforms, multi-frequency, periodic phenomena, fluid flow, online analysis, turbomachinery

Summary. Unsteady flow simulations in the time-domain are attractive for evaluating several phenomena. All unsteady effects can be directly captured in such simulations. Nevertheless, it remains a challenge in such time-domain simulations to extract the frequency content efficiently. This is especially true when incommensurable frequencies are present in a simulation. To address this problem, in this work we investigate the application of Almost Periodic Fourier Transforms (APFTs) to compute the harmonic content of time-domain simulations online. APFTs do not require the definition and use of a beat frequency and therefore often require significantly fewer sample points, allowing the discrete spectra of transient simulations to be determined faster and with less numerical effort. In this paper, we give a brief introduction to the APFT methodology and describe its implementation in a CFD code. To investigate and demonstrate the application of the method, we consider two academic test cases: the advection of an entropy disturbance in an empty duct and the interaction of an artificial vorticity disturbance with an oscillating compressor blade, which corresponds to the well-known aeroelasticity test case Standard Configuration 10.

1 INTRODUCTION

In modern multidisciplinary turbomachinery component design, unsteady flow simulations are essential to understand topics such as flutter, noise generation or blade-row interactions. Although (nonlinear) frequency-based methods can often be used for such applications, these methods typically require a detailed knowledge of the frequency content of the unsteady flow field. However, since blade-row interaction in multistage turbomachinery components can lead to a plethora of solution harmonics, a complete specification of these frequencies is not always feasible. In this context, time-domain simulations are attractive since an a priori specification of the solution harmonics is not required and all unsteady effects can be directly captured within the limits of the simulation duration and time step size. Nevertheless, it remains a challenge

in such time-domain simulations to extract the frequency content efficiently. This is especially true when incommensurable frequencies are present in a simulation. To address this problem, in this work we investigate the application of Almost Periodic Fourier Transforms (APFTs) to compute the harmonic content of time-domain simulations online. This is the basis for the efficient simulation of configurations in which two or more fundamental frequencies occur that are not harmonics of each other. In contrast to a conventional Discrete Fourier Analysis (DFT), APFTs do not require the definition and use of a beat frequency and therefore often require significantly fewer sample points, so that the discrete spectra of unsteady simulations can be determined faster and with less numerical effort. In this paper, we give a brief introduction to the APFT methodology for such problems and describe its implementation in the CFD code TRACE (see [1], [2] and [3]). TRACE is a parallel Navier-Stokes flow solver for structured and unstructured grids developed at the DLR Institute of Propulsion Technology in close cooperation with MTU Aero Engines AG. The code uses the finite volume discretization of the compressible unsteady Favre- and Reynolds-averaged Navier-Stokes equations in the relative reference frame in a highly parallelized framework using a multiblock approach and modern communication structures. Inviscid fluxes are calculated using Roe's flux-difference-splitting method. The upwind states are computed using the monotone upstream-centered scheme for conservation laws with a modified van Albada limiter to smooth the solution near shocks. The viscous terms are discretized with accurate second-order central differences.

In this work several adjustments were made to the flow solver, including CGNS Fourier output, non-reflective Fourier boundary conditions, 0D and 1D averages at interfaces, and sample data used in online post-processing. The use of APFTs also allows Fourier decomposition of arbitrary frequencies (including non-multiples of the base frequency) in such simulations. This allows the time interval for averaging to be shortened, which reduces the calculation time.

To investigate and demonstrate the application of the method we consider two academic test cases: the advection of an entropy disturbance in an empty duct, and the interaction of an artificial vorticity disturbance with an oscillating compressor blade corresponding to the well-known aeroelasticity test case Standard Configuration 10.

2 THEORY

The APFT was introduced by Kundert et al. [4] in the analysis of near-periodic microwave circuits in the frequency-domain. In this section, the theory is presented. Furthermore, the problem of non-orthogonality and the condition number is discussed and a solution approach is presented.

2.1 Construction of an APFT-Matrix

While the frequency spectrum is defined by the signal length and the sampling theorem in the DFT, the frequencies to be analyzed and the sampling length can be defined in the APFT itself. For the arbitrary frequencies $f_1, f_2, \ldots, f_L$ and the sampling length N, the reconstruction

in the time-domain is defined as follows:

$$\mathbf{A} \cdot \begin{pmatrix} \hat{a}_0 \\ \Re(\hat{a}_1) \\ -\Im(\hat{a}_1) \\ \vdots \\ \Re(\hat{a}_L) \\ -\Im(\hat{a}_L) \end{pmatrix} = \begin{pmatrix} u(t_1) \\ u(t_2) \\ u(t_3) \\ \vdots \\ u(t_N) \end{pmatrix} \tag{1}$$

The matrix of the inverse APFT (iAPFT) is thus:

$$\mathbf{A}^{-1} = \begin{pmatrix} 1 & \cos\omega_1 t_1 & \sin\omega_1 t_1 & \cdots & \cos\omega_L t_1 & \sin\omega_L t_1 \\ 1 & \cos\omega_1 t_2 & \sin\omega_1 t_2 & \cdots & \cos\omega_L t_2 & \sin\omega_L t_2 \\ 1 & \cos\omega_1 t_3 & \sin\omega_1 t_3 & \cdots & \cos\omega_L t_3 & \sin\omega_L t_3 \\ \vdots & \vdots & \vdots & \ddots & \vdots & \vdots \\ 1 & \cos\omega_1 t_N & \sin\omega_1 t_N & \cdots & \cos\omega_L t_N & \sin\omega_L t_N \end{pmatrix} \tag{2}$$

Battistoni et al. [5] applied the APFT to analyze the time series of an unsteady flow of a two-spool turbomachine. The sampling length N is the length of the vector of sample points. As this is usually significantly greater than the number of frequencies L, the matrix is not square and therefore no longer orthogonal. The use of a classical matrix inversion is not possible. There are various methods for calculating the so-called Moore-Penrose inverse. The singular value decomposition with the numerical linear algebra library LAPACK [6] is used here. When defining the frequency set, the sampling theorem for the time step size of the present signal must also be taken into account.

2.2 Condition number

With the before mentioned non-orthogonality of the APFT-matrix, the condition number of this matrix becomes an issue, we have to address. The condition number κ represents a quantity for the maximum amplification of the error when solving a linear system of equations with the coefficient matrix $\mathbf{A}$ as a function of the relative error of the input data. It is defined by

$$\kappa = \frac{\sigma_{max}(\mathbf{A})}{\sigma_{min}(\mathbf{A})}. \tag{3}$$

Here, $\sigma_{\min}/\sigma_{\max}$ is the minimum/maximum singular value of $\mathbf{A}$. This results in some restrictions for the sampling interval and the fundamental frequencies should not be too close to each other or differ significantly. In their investigation, Battistoni et al. [5] set an upper limit of the condition number of 2 for an automatic detection of frequencies. A reduction of the condition number is only possible by increasing the sampling length or removing critical frequencies from the frequency set. However, removing frequencies can lead to a poor representation of the problem under consideration and is therefore not possible in some cases or has a negative effect on the results. To overcome this drawback of the APFT, the approach of Li and Ekici [7] was adapted to compute the Moore-Penrose inverse. They introduced the concept of supplemental frequencies together with the primary frequencies.

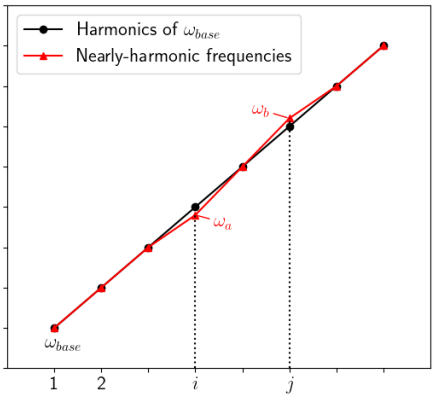

Figure 1: Example of supplemental-frequency APFT

Starting with a harmonic expansion of an unknown ω_{Base} as follows:

$$[\omega_{Base}, 2\omega_{Base}, \ldots, i\omega_{Base}, \ldots, j\omega_{Base}, \ldots] \tag{4}$$

Now we can replace the harmonics that are close to the frequencies of interest ω_a and ω_b.

$$\begin{aligned} i\omega_{Base} &\approx \omega_a, \text{ so that } i\omega_{Base} \leftarrow \omega_a \\ j\omega_{Base} &\approx \omega_b, \text{ so that } j\omega_{Base} \leftarrow \omega_b \end{aligned} \tag{5}$$

The result is a new, nearly-harmonic frequency array that contains not only the frequencies we are interested in, but also additional frequencies.

$$[\omega_{Base}, 2\omega_{Base}, \ldots, \omega_a, \ldots, \omega_b, \ldots] \tag{6}$$

A new base frequency is determined so that the frequency set, consisting of the primary frequencies together with additional frequencies, forms a nearly-harmonic series. This leads to a small condition number for the APFT matrix, which should have a direct effect on stability. The procedure is illustrated in Figure 1.

To determine the appropriate ω_{Base}, a line search optimization is used to reduce the condition number of the supplemental-frequency APFT-matrix. After forming the Moore-Penrose inverses, these additional frequencies can be ignored. Although this leads to an increased numerical effort in the formation of the APFT matrix, it does not affect its application.

3 APPLICATION OF ALMOST PERIODIC FOURIER TRANSFORMATIONS

The APFT described in section 2 can be applied in TRACE in various ways. For online monitoring, you have the option of defining a virtual probe point at which the flow can be stored and analyzed. These probe points also provide a Fourier decomposition of the recorded flow. The APFT can be used here to flexibly analyze multi-frequency problems. With the APFT defined, the entire flow field can also be transformed and the resulting Fourier coefficients can be stored in CGNS format for later analysis. The APFT can also offer advantages in the formation

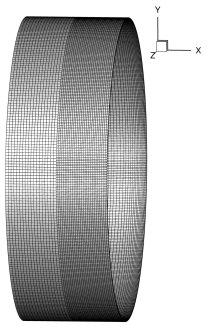

(a) Mesh of a thin empty channel

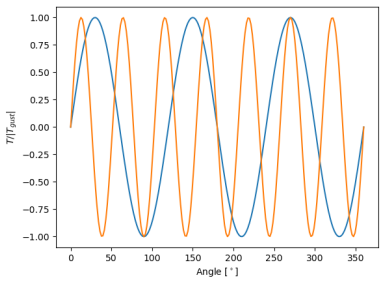

(b) Circumferential Disturbances at the inlet

Figure 2: Configuration of the empty duct with entropy disturbances

of 0D and 1D averages at interfaces. Instead of using a very long averaging time based on a common fundamental frequency, an APFT can calculate these values in a much shorter time. These averaged values at the interfaces are not only relevant as a result of the simulation, but also have a direct influence on the simulation as the boundary conditions define the operating point of the configuration based on these values. In this way, the time interval for averaging can be shortened with respect to selected frequencies, reducing the calculation time. To test and verify the APFT implementation in TRACE, two cases of academic nature were considered. These are now briefly presented.

3.1 Entropy Disturbances in Empty Duct

The first test case is an empty duct with a constant mean flow. In the radial direction, it consists of only one cell layer. The mesh consists of ≈ 22000 cells shown in Figure 2a. The mesh is treated as stationary in the front part and as rotating at 3000 RPM in the rear, finer part. At the inlet of the duct, circumferential temperature perturbations of 10K are prescribed. These disturbances are the 3rd and 7th circumferential modes of frequency $f_{Gust} = 500\text{Hz}$. As can be seen in Figure 2b, the two disturbances are only periodic after 360°.

A mode transformation of the prescribed disturbances into the rotating system using

$$\omega' = \left|\omega + m\left(\Omega' - \Omega\right)\right| \tag{7}$$

$$m' = \begin{cases} m, & \text{if } \omega + m\left(\Omega' - \Omega\right) \geq 0 \\ -m, & \text{if } \omega + m\left(\Omega' - \Omega\right) < 0 \end{cases} \tag{8}$$

gives the expected frequencies.

$$\begin{aligned} f_1 &= 650\text{Hz} \\ f_2 &= 850\text{Hz} \end{aligned} \tag{9}$$

In the rotating system of the duct, these disturbances have a small common fundamental frequency.

$$f_{Base} = 50\text{Hz} \tag{10}$$

In Figure 3a you can see an instantaneous snapshot of the temperature field resulting from the two inlet perturbations.

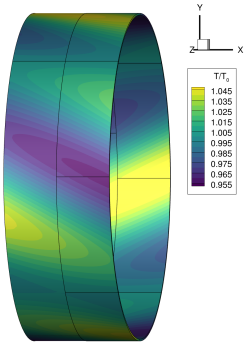

(a) Temperature field with the both modes

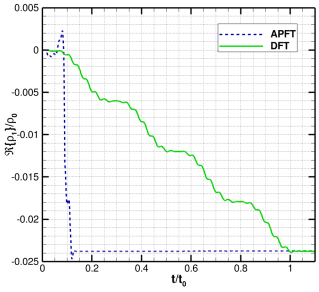

(b) Development of the normalized real part of the Fourier coefficient of the density of $f_1 = 650$Hz at the outlet

Figure 3: Use of the APFT in an empty duct with two modes

The aim here is to determine the mean value with as few physical time steps as possible. Figure 3b shows the temporal development of the normalized real part of the Fourier coefficient of the density of $f_1 = 650$Hz at the outlet. While a DFT (green) requires a whole period of the common fundamental frequency to determine a time-averaged value, an APFT (dashed blue) can do this much faster. In this case, the DFT uses the full 640 time steps, while the APFT requires only 50 time steps. As mentioned above, the APFT is also used to create a Fourier decomposition of the entire flow field. Figure 4a shows the normalized real part of the Fourier coefficient of the density of $f_1 = 650$Hz in the rotating system of the converged state. Figure 4b shows the development of the time average of the density at the outlet. Again, the use of the APFT approach leads to a significant reduction in the number of sampling points required to calculate the time average. The figure also contains a zoom on the converged part of the time series. When using the APFT approach, small amplitude perturbations are visible in the time-mean value of density. There may be several explanations for this, e.g. missing frequencies in the APF matrix, too few sampling points or a high condition number. The most likely explanation here seems to be the overly aggressive choice of sampling points.

3.2 Modified Standard Configuration 10 Case 2

To demonstrate the ability of the APFT approach to simultaneously capture unsteady disturbances at arbitrary excitation frequencies, the well-established aeroelasticity test configuration 10 is investigated in the presence of an artificial inflow disturbance that mimics an upstream blade wake. The results presented here refer to the Standard Configuration 10, a two-dimensional compressor cascade consisting of modified NACA006 airfoils and operating at subsonic inlet and outlet conditions. The geometric details can be found in Table 1. A subsonic operating point is calculated for all simulations. The resulting boundary conditions are specified in Table 2. Detailed information about the profile geometry and boundary conditions can be found in the publications of Bölcs and Fransson [8] and Fransson and Verdon [9]. The pitching mode used here as blade motion is referred to by the authors as “Case 2” and is defined about a pitching

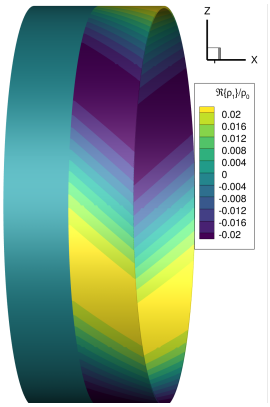

(a) Normalized real part of the Fourier coefficient of the density of $f_1 = 650$Hz in rotating system

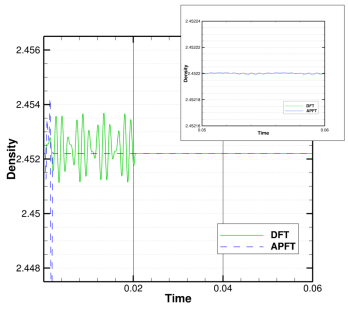

(b) Development of density time mean at outlet including a zoomed section to the converged state

Figure 4: Results obtain by using the APFT approach with an empty duct

Table 1: Geometric setup of Standard Configuration 10

Periodicity	translational
Pitch	1m
Chord	1m
Height	0.03m
Stagger angle	45°
Pitching axis	$(0.5, 0.05)$
Torsion angle	0.1°

Table 2: Subsonic mean flow conditions of Standard Configuration 10

Inlet Mach number	0.7
Inflow angle	55°
Inflow total pressure	101325Pa
Inflow total temperature	288.15K
Inflow velocity	227.287m/s
Inflow pressure	73047.5Pa
Outflow pressure	88250Pa

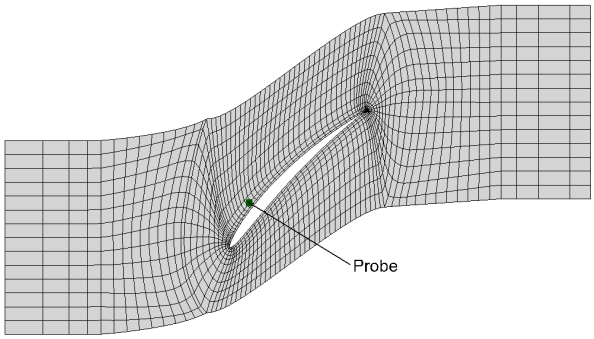

Figure 5: Simulation domain of one passage of Standard Configuration 10 (every second grid line shown) with probe location

axis defined on the camber line at midchord and the stagger angle γ

$$\begin{pmatrix} x_0 \\ y_0 \end{pmatrix} = \begin{pmatrix} \cos\gamma & \sin\gamma \\ \sin\gamma & \cos\gamma \end{pmatrix} \begin{pmatrix} 0.5 \\ 0.05 \end{pmatrix}. \tag{11}$$

An amplitude of $\alpha = 0.1°$ is chosen for the pitching. It is expected that the response of the flow is almost linear at this amplitude. In this work, case 2 with an interblade phase angle of $\sigma = 90°$ and a reduced frequency

$$k = \frac{\omega c}{v_{Inlet}} = 0.5 \tag{12}$$

has been simulated. Therefore, the resulting eigenmode with the given boundary conditions is

$$f_{Eigenmode} = \frac{k v_{Inlet}}{2\pi c} = 18.094822\text{Hz}. \tag{13}$$

In order to generate a multi-frequency problem, an artificial wake is prescribed at the inlet and the interaction with the blade oscillation is analyzed.

$$u(\vartheta, t) = \overline{u} + u'(\vartheta), \text{ with } u'(\vartheta) = U e^{i(\omega t + m\vartheta)} \tag{14}$$

The wake is defined as a sinusoidal time-periodic velocity disturbance with the circumferential wave number $m = \pi$. The complex amplitude of the disturbance is set to 10% of the time-averaged velocity. In order to be able to compare the results of the APFT with a standard DFT based on the greatest common divisor of the occurring frequencies, the ratio between the two base frequencies is chosen so that it is in an appropriate ratio. To mimic the case where the frequencies have a small greatest common divisor compared to the frequencies of interest, the ratio between the two fundamental frequencies is set to

$$\frac{f_{Eigenmode}}{f_{Wake}} = \frac{22}{7} \tag{15}$$

which is a rational approximation to π. The results were obtained for an inviscid flow on a coarse 2D grid with 5600 cells Figure 5 and serve to validate the numerical algorithm.

Three different simulations were carried out for this test case. A time-domain simulation using a classical DFT, with the Greatest Common Divisor of the two frequencies used as the

fundamental frequency. To extract the frequency content of the simulation, 2272 sampling points and 71 frequencies were used. These 71 frequencies consist of the harmonics of the two fundamental frequencies and their linear combinations. This simulation is used as a reference in the following. Secondly, a time-domain simulation is carried out with the APFT presented here. Here, only 1590 sampling points are used and only the relevant 22 selected frequencies. Thirdly, a simulation in the frequency-domain was carried out using a multidimensional Fourier transform (MDFT). Details on the implementation and validation of the Harmonic Balance method using MDFTs can be found in Junge et al. [10]. In this simulation, the same 22 frequencies were used as in the time-domain simulation using APFT.

Figure 6 shows snapshots of the instantaneous Mach number distribution over the domain. The snapshots were reconstructed in the time-domain using the Fourier coefficients calculated with the various methods outlined previously. For the sake of clarity, the simulation in the single-passage frequency-domain has been plotted on multiple passages in a post-processing step. In addition, the amplitude $\alpha = 0.1^\circ$ of the pitching motion was amplified by a factor of 90 to emphasize the movement of the blades. The prescribed wake enters the calculation area on the left-hand side of the domain. After convection through the inlet area, the wake vortices hit the suction side of every other blade. At the leading edge of the blades, the interaction of the incoming unsteady disturbance with the surface of the blade creates a local region where the flow state becomes transonic. The additional black contour line shows the instantaneous $Ma = 1$ region, which varies in the translational direction due to the different phase positions of the blades. Although an almost linear flow behavior can be expected for the selected amplitude of the pitching motion, the incoming vortices introduce a time-periodic flow with a strong nonlinear interaction with the moving blade. The comparison shows very good agreement between all three simulations. The convection of the incoming wake vortex is captured almost identically, and the existence of the local transonic flow caused by the interaction of wake vortex and blade is confirmed by all simulations.

The development of the Fourier coefficients in the two time-domain simulations at the probe position is shown in Figure 7. The APFT is able to accurately capture the frequency content with $\approx 70\%$ sampling points and a significantly reduced frequency set. As a result, the APFT simulation reaches the convergent state faster.

Figure 8 shows the unsteady imaginary pressure coefficient $\Im\{\hat{c}_{p,\omega}\}/\alpha$ of the first harmonic of the eigenmode frequency for different simulation methods in the presence of the artificial wake. At a relative chord length $s/c = 0.2$, the simulations resolve a clear pressure coefficient drop with a strong gradient on the suction side of the blade. It can be seen that the time-domain simulation resolves the pressure drop equally well. The APFT is able to resolve this strong non-linearity with a smaller number of sampling points and frequencies. The Harmonic Balance simulation with the MDFT produces overshoots in the transonic region and the peak amplitude is slightly shifted downstream.

4 CONCLUSIONS

The results show that it is possible to efficiently simulate multi-frequency problems with an arbitrary frequency ratio in the time-domain. The use of APFTs for this purpose shows great potential for arbitrary multi-frequency problems. It is an excellent tool for analyzing in the frequency-domain and for achieving convergence acceleration even in the presence of

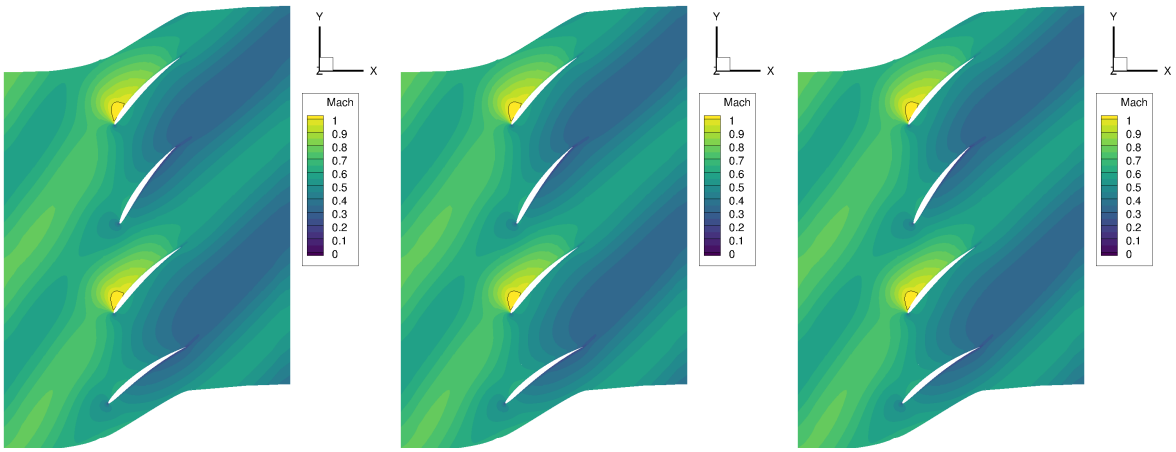

(a) Time-domain simulation using DFT (b) Time-domain simulation using APFT (c) Harmonic balance simulation using MDFT

Figure 6: Reconstructed instantaneous Mach number

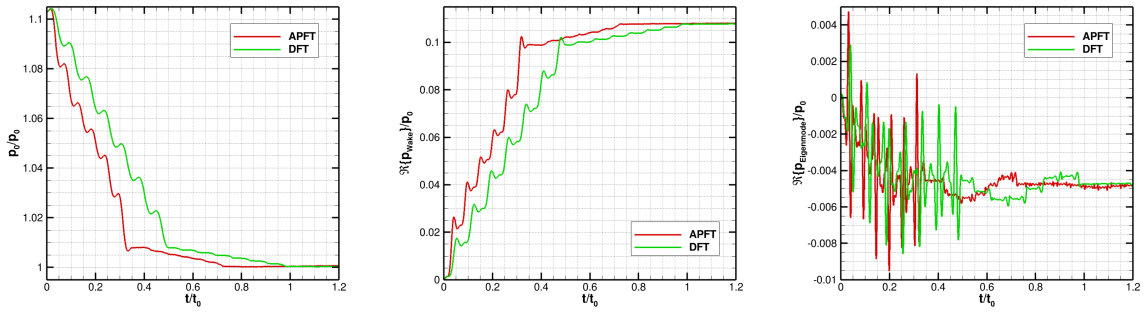

(a) Mean flow (b) Artificial wake (c) Pitching motion

Figure 7: Development of relevant Fourier coefficients at probe

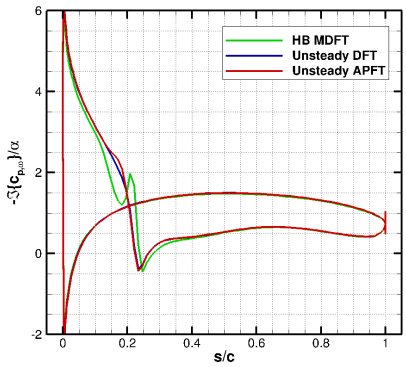

Figure 8: Unsteady imaginary pressure coefficient of eigenmode (local damping coefficient)

incommensurable frequencies. However, the construction of an APFT is not trivial. Several aspects must be taken into account. In most complex simulations, the set of frequencies is unknown a-priori. Together with too few sampling points and a very high condition number of the APFT-matrix, this can have a major impact on the quality of the online Fourier analysis.

References

[1] K. Becker, K. Heitkamp, and E. Kügeler, "Recent progress in a hybrid-grid CFD solver for turbomachinery flows," in *Proceedings Fifth European Conference on Computational Fluid Dynamics ECCOMAS CFD 2010*, Lisbon, Portugal, Jun. 2010. [Online]. Available: http://congress2.cimne.com/eccomas/proceedings/cfd2010/papers/01609.pdf.

[2] G. Geiser, J. Wellner, E. Kügeler, A. Weber, and A. Moors, "On the simulation and spectral analysis of unsteady turbulence and transition effects in a multistage low pressure turbine," *Journal of Turbomachinery*, vol. 141, no. 5, p. 051 012, Jan. 2019, ISSN: 0889-504X. DOI: 10.1115/1.4041820.

[3] M. Bergmann, C. Morsbach, B. F. Klose, G. Ashcroft, and E. Kügeler, "A numerical test rig for turbomachinery flows based on large eddy simulations with a high-order discontinuous galerkin scheme – part i: Sliding interfaces and unsteady row interactions," *Journal of Turbomachinery*, vol. 146, no. 2, p. 021 005, Nov. 2023, ISSN: 0889-504X. DOI: 10.1115/1.4063734.

[4] K. S. Kundert, G. B. Sorkin, and A. Sangiovanni-Vincentelli, "Applying harmonic balance to almost-periodic circuits," *IEEE Transactions on Microwave Theory and Techniques*, vol. 36, no. 2, pp. 366–378, 1988. DOI: 10.1109/22.3525.

[5] C. Battistoni, H. Müller, N. Wolfrum, and G. Ashcroft, "Numerical simulation of turbomachinery flows considering two-spool effects: Application of the almost-periodic fourier transform," in *AIAA SCITECH 2022 Forum*. 2022. DOI: 10.2514/6.2022-0490. eprint: https://arc.aiaa.org/doi/pdf/10.2514/6.2022-0490.

[6] E. Anderson, Z. Bai, C. Bischof, S. Blackford, J. Demmel, J. Dongarra, J. Du Croz, A. Greenbaum, S. Hammarling, A. McKenney, and D. Sorensen, *LAPACK Users' Guide*, Third. Philadelphia, PA: Society for Industrial and Applied Mathematics, 1999, ISBN: 0-89871-447-8.

[7] H. Li and K. Ekici, "Supplemental-frequency harmonic balance: A new approach for modeling aperiodic aerodynamic response," *Journal of Computational Physics*, vol. 436, p. 110 278, 2021, ISSN: 0021-9991. DOI: 10.1016/j.jcp.2021.110278. [Online]. Available: https://www.sciencedirect.com/science/article/pii/S002199912100173X.

[8] A. Bölcs and T. H. Fransson, *Aeroelasticity in Turbomachines: Comparison of Theoretical and Experimental Cascade Results*, ser. Communication du Laboratoire de thermique appliquée de l'Ecole polytechnique fédérale de Lausanne. ECOLE POLYTECHNIQUE FEDERALE DE LAUSANNE (Switzerland) LAB DE THERMIQUE APPLIQUEE, 1986.

[9] T. H. Fransson and J. M. Verdon, "Updated report on standard configurations for the determination of unsteady flow through vibrating axial-flow turbomachine-cascades," in *Report Royal Institute of Technology, Stockholm, Sweden*, 1991. [Online]. Available: https://www.rpmturbo.com/testcases/STCF/STCF1to10/Documents/SC2110.92update.pdf.

[10] L. Junge, C. Frey, G. Ashcroft, and E. Kügeler, "A new harmonic balance approach using multidimensional time," *Journal of Engineering for Gas Turbines and Power*, vol. 143,

no. 8, p. 081 007, Mar. 2021, ISSN: 0742-4795. DOI: 10.1115/1.4049698. eprint: https://asmedigitalcollection.asme.org/gasturbinespower/article-pdf/143/8/081007/6674770/gtp_143_08_081007.pdf.